JOURNAL OF COMPUTATIONAL PHYSICS 89, 389–413 (1990)

An Efficient Scheme for Solving Steady Incompressible Navier–Stokes Equations

CHARLES-HENRI BRUNEAU AND CLAUDE JOURON

Université Paris-Sud, Laboratoire d'Analyse Numérique, Bâtiment 425, 91405 Orsay, France

Received September 9, 1988; revised August 3, 1989

The steady incompressible Navier–Stokes equations in a 2D driven cavity are solved in primitive variables by means of the multigrid method. The pressure and the components of the velocity are discretized on staggered grids, a block-implicit relaxation technique is used to achieve a good convergence and a simplified FMG-FAS algorithm is proposed. Special focus on the finite differences scheme used to approach the convection terms is made and a large discussion with other schemes is given. Results in a square driven cavity are obtained for Reynolds numbers as high as 15,000 on fine uniform meshes and the solution is in good agreement with other studies. For $Re = 5000$ the secondary vortices are very well represented showing the robustness of the method. For Reynolds numbers higher than 5000 the loss of stability for the steady solution is discussed. Moreover, some computations on a rectangular cavity of aspect ratio equal to two are presented. In addition the method is very efficient as far as CPU time is concerned; for instance, the solution for $Re = 1000$ on a 128×128 grid is obtained within 24 s on a SIEMENS VP 200.

INTRODUCTION

In the seventies, following some first works such as [1], many numerical methods were studied to solve the incompressible Navier–Stokes equations. These methods gave first indications on the shape of the solutions for Reynolds numbers up to 1000 but where limited by the lack of capacity of the computers. A quite exhaustive survey can be found in [2, 3]. Today with the development of powerful computers with large memory and vector processors a new era of scientific computing is coming. In particular one can expect to make significant progress involving Navier–Stokes equations, to observe the transition to turbulence as done in [4], and in the future to compute turbulent flows; according to Kolmogorov and [5], this will need as many degrees of freedom as $Re^{9/4}$ in three dimensions. Such an amount of grid points for a high Reynolds number requires huge memory which is not available yet; but some work can already be done, in particular, in two dimensions. In this work we solve steady flows in a driven cavity and our aim is to observe, on one hand, solutions exhibiting good representation of secondary vortices for large Reynolds numbers and, on the other hand, the transition to turbulence.

Many approaches have been proposed this last decade to compute solutions of

0021-9991/90 $3.00

Navier–Stokes equations, among them the spectral method, the linearization methods and the multigrid method. The spectral or pseudo-spectral methods give good results for natural convection (see, for instance, [6] and references therein). They can also be used for the regularized driven cavity problem [7]. The linearization by Newton's method either with a velocity-pressure formulation [4] or with a stream function-vorticity formulation [8] and finally the multigrid method in primitive variables [9] or in flow variables [10] are currently used. All these methods yield about the same steady solution for $Re = 1000$ and some good solutions for Re as high as 5000 or 10,000; nevertheless for these high Reynolds numbers there are some noticeable discrepancies from one method to an other.

In brief we can say that everyone agrees on the main characteristics of the flow in a square cavity: the presence of a large primary vortex the center of which moves to the center of gravity of the square cavity as Re increases, the apparition of secondary vortices in the bottom corners and then in the corner of the incoming flow, the formation of quite large tertiary corner vortices for high Reynolds numbers [11]. But there is quite poor representation of these small structures in the corners and along the walls of the cavity. In [12] a local grid refinement procedure permits to capture, in a bottom corner, Moffat vortices with geometric progression scaling in good agreement with the theory; this shows that small phenomena occuring in the boundary layer can be obtained by numerical methods if there are enough points to represent them. The questions are: are there other eddies than Moffat eddies? And if there are other eddies, where are they located, how do they appear when the Reynolds number increases, and what is their role in the route to turbulence?

In this work we try to give an answer to this question by computing the solution on fine grids for high Reynolds numbers in a square driven cavity and in a rectangular one of aspect ratio two; the comparison of these two cases shows that some difficulties, occurring in the square driven cavity for $Re > 5000$, can appear already for $Re = 1000$ in the rectangular one where the flow is much more unstable [13].

After some recalls on the equations, we present in this paper a FMG-FAS (full multigrid–full approximation storage) algorithm with simplified control tests and use the SCGS (symmetrical coupled Gauss–Seidel) smoothing procedure proposed in [9]. Then we study several finite difference schemes approximating the convection terms and show the influence of local testing of the velocity sign on one hand and second-order uncentered approximation of derivatives on the other hand to get an efficient scheme. Here, by efficient, we mean that the scheme is able to represent the solution as soon as there are enough points in the boundary layer. Finally we give results on grids as fine as 512×512 and a range of Reynolds number between 100 and 15,000 for the square cavity and between 100 and 1000 for the rectangular cavity of aspect ratio two. The results are compared with those obtained in [8–10, 14] for Reynolds numbers less than or equal to 5000. For higher Reynolds numbers we observe the appearance of small eddies along the walls and conjecture that they play a significant role in the transition to turbulence.

1. Mathematical Problem and Approximation

The non-dimensional Navier–Stokes equations of an incompressible viscous fluid in two dimensions are written as follows in primitive variables,

$$\begin{aligned} -\frac{1}{\mathrm{Re}}\Delta u + u\frac{\partial u}{\partial x} + v\frac{\partial u}{\partial y} + \frac{\partial p}{\partial x} &= 0 \\ -\frac{1}{\mathrm{Re}}\Delta v + u\frac{\partial v}{\partial x} + v\frac{\partial v}{\partial y} + \frac{\partial p}{\partial y} &= 0 \\ \frac{\partial u}{\partial x} + \frac{\partial v}{\partial y} &= 0, \end{aligned} \tag{1.1}$$

where $\mathbf{q} = (u, v)^\top$ and p denote the velocity and the pressure, respectively. The Reynolds number we speak of in this paper is the one appearing in equations (1.1) although it is representative neither of the macro structures nor of the micro structures; but it is better to take this one to compare with other authors. This work concerns only the well-known driven cavity problem, so Eqs. (1.1) are set in a domain $\Omega = (0, 1) \times (0, b)$ with $b = 1$ or 2 and are associated to the following Dirichlet boundary conditions:

$$\begin{aligned} u &= 1 \quad \text{on} \quad I = (0, 1) \times \{b\} \\ u &= 0 \quad \text{on} \quad \partial\Omega \backslash I \\ v &= 0 \quad \text{on} \quad \partial\Omega. \end{aligned} \tag{1.2}$$

Once again one could contest such a discontinuous boundary condition for u, in particular with spectral method $u = 1$ would be replaced by $u = (1 - (2x - 1)^2)^2$, for instance, but for comparison we take condition (1.2) even if it is not the best one; moreover, this discontinuity is not the main difficulty. Indeed the difficulties are, as it is well known, the representation of the pressure defined within an arbitrary constant and the treatment of the non-linear convection terms. We shall see in the next sections how to avoid the first difficulty and how to treat the second one.

Let us rewrite Eqs. (1.1) in the form

$$\begin{aligned} N(u, v) + \nabla p &= 0 \\ \mathrm{Div}\, \mathbf{q} &= 0, \end{aligned} \tag{1.3}$$

where $N(u, v)$ is the sum of linear diffusion terms $D(u, v)$ and non-linear convection terms $C(u, v)$; we approximate these operators by finite differences on staggered grids with the pressure given at the center of a cell and the components of the velocity given at the middle of the sides as usual (see Fig. 1).

Let G_l be the fine grid on which we are looking for the solution; we use centered finite differences to approximate the linear terms. So on the cell (i, j) we have for the variables $u_{i-1/2,j}$, $v_{i,j-1/2}$, and $p_{i,j}$ the formulas,

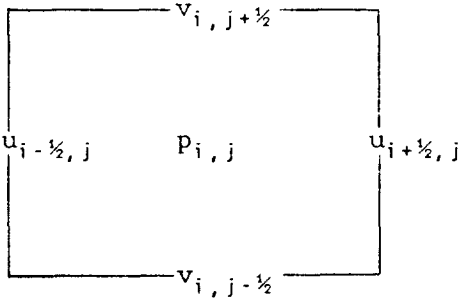

FIG. 1. Pressure and velocity in the cell (i, j).

$$[D_l(u,v)]_{(i,j)} = \begin{cases} \dfrac{1}{\mathrm{Re}(\Delta x)^2}(2u_{i-1/2,j} - u_{i+1/2,j} - u_{i-3/2,j}) \\ \qquad + \dfrac{1}{\mathrm{Re}(\Delta y)^2}(2u_{i-1/2,j} - u_{i-1/2,j+1} - u_{i-1/2,j-1}) \\ \dfrac{1}{\mathrm{Re}(\Delta x)^2}(2v_{i,j-1/2} - v_{i+1,j-1/2} - v_{i-1,j-1/2}) \\ \qquad + \dfrac{1}{\mathrm{Re}(\Delta y)^2}(2v_{i,j-1/2} - v_{i,j+1/2} - v_{i,j-3/2}) \end{cases}$$

$$[\nabla_l p]_{(i,j)} = \begin{cases} \dfrac{1}{\Delta x}(p_{i,j} - p_{i-1,j}) \\ \dfrac{1}{\Delta y}(p_{i,j} - p_{i,j-1}) \end{cases} \tag{1.4}$$

$$[\mathrm{Div}_l \mathbf{q}]_{(i,j)} = \frac{1}{\Delta x}(u_{i+1/2,j} - u_{i-1/2,j}) + \frac{1}{\Delta y}(v_{i,j+1/2} - v_{i,j-1/2}),$$

where u, v, p are the discretized variables on the grid G_l and Δx and Δy are the size of the uniform mesh in the x and y direction, respectively.

In addition we propose in this paper to approximate the nonlinear convection term $[C_i(u,v)]_{(i,j)}$ as follows for the first component:

$$\begin{cases} \dfrac{u_{i-1,j}^{n-1}}{3\Delta x}(4u_{i-1/2,j} - 5u_{i-3/2,j}^{n-1} + u_{i-5/2,j}^{n-1}) & \text{if } u_{i-1,j}^{n-1} > 0 \\ -\dfrac{u_{i,j}^{n-1}}{3\Delta x}(4u_{i-1/2,j} - 5u_{i+1/2,j}^{n-1} + u_{i+3/2,j}^{n-1}) & \text{if } u_{i,j}^{n-1} < 0 \end{cases} \tag{1.5a}$$

$$+ \begin{cases} \dfrac{v_{i-1/2,j-1/2}^{n-1}}{3\Delta y}(4u_{i-1/2,j} - 5u_{i-1/2,j-1}^{n-1} + u_{i-1/2,j-2}^{n-1}) & \text{if } v_{i-1/2,j-1/2}^{n-1} > 0 \\ -\dfrac{v_{i-1/2,j+1/2}^{n-1}}{3\Delta y}(4u_{i-1/2,j} - 5u_{i-1/2,j+1}^{n-1} - u_{i-1/2,j+2}^{n-1}) & \text{if } v_{i-1/2,j+1/2}^{n-1} < 0 \end{cases}$$

and for the second component:

$$\begin{cases} \dfrac{u^{n-1}_{i-1/2,j-1/2}}{3\,\Delta x}\,(4v_{i,j-1/2} - 5v^{n-1}_{i-1,j-1/2} + v^{n-1}_{i-2,j-1/2}) & \text{if } u^{n-1}_{i-1/2,j-1/2} > 0 \\ -\dfrac{u^{n-1}_{i+1/2,j-1/2}}{3\,\Delta x}\,(4v_{i,j-1/2} - 5v^{n-1}_{i+1,j-1/2} + v^{n-1}_{i+2,j-1/2}) & \text{if } u^{n-1}_{i+1/2,j-1/2} < 0 \end{cases} \tag{1.5b}$$

$$+ \begin{cases} \dfrac{v^{n-1}_{i,j-1}}{3\,\Delta y}\,(4v_{i,j-1/2} - 5v^{n-1}_{i,j-3/2} + v^{n-1}_{i,j-5/2}) & \text{if } v^{n-1}_{i,j-1} > 0 \\ -\dfrac{v^{n-1}_{i,j}}{3\,\Delta y}\,(4v_{i,j-1/2} - 5v^{n-1}_{i,j+1/2} + v^{n-1}_{i,j+3/2}) & \text{if } v^{n-1}_{i,j} < 0. \end{cases}$$

We shall see in detail in Section 4 how this scheme is constructed. We cannot do it now because we need to describe the relaxation solver first.

In summary we get a nonlinear finite dimensional operator L_l and we have to solve:

$$L_l(u, v, p) = 0 = f_l. \tag{1.6}$$

2. Multigrid Procedure

In order to solve (1.6) we use a FMG-FAS algorithm. So that this paper may be relatively self-contained we briefly described these multigrid procedures; for more details the reader is refered to [15, 16]. The Full Approximation Storage algorithm consists in evaluating a residue, projecting this residue on a coarser grid, computing a corrector on this coarse grid, then extending this corrector to the fine grid, and correcting the previous solution. One step can be summarized for a linear problem on two consecutive grids, G_k and G_{k-1},

$$\begin{cases} \text{Solve } L_k(u_k, v_k, p_k) = f_k \\ r_k = f_k - L_k(u_k, v_k, p_k) \\ f_{k-1} = P^k_{k-1} r_k \\ \text{Solve } L_{k-1}(u_{k-1}, v_{k-1}, p_{k-1}) = f_{k-1} \\ (u_k, v_k, p_k) \leftarrow (u_k, v_k, p_k) + E^{k-1}_k(u_{k-1}, v_{k-1}, p_{k-1}), \end{cases} \tag{2.1}$$

where (u_k, v_k, p_k) denote the variables on the grid G_k, P^k_{k-1} is the projection operator from the grid G_k to the grid G_{k-1} and E^{k-1}_k is the extension operator from the grid G_{k-1} to the grid G_k. For a nonlinear problem the algorithm is slightly different and can be written in the form:

$$\begin{cases} \text{Solve } L_k(u_k, v_k, p_k) = f_k \\ r_k = f_k - L_k(u_k, v_k, p_k) \\ f_{k-1} = P_{k-1}^k r_k + L_{k-1}(P_{k-1}^k(u_k, v_k, p_k)) \\ \text{Solve } L_{k-1}(u_{k-1}, v_{k-1}, p_{k-1}) = f_{k-1} \\ (u_k, v_k, p_k) \leftarrow (u_k, v_k, p_k) + E_k^{k-1}((u_{k-1}, v_{k-1}, p_{k-1}) - P_{k-1}^k(u_k, v_k, p_k)). \end{cases} \tag{2.2}$$

For a set of grids $(G_k)_{k=1,\ldots,l}$ the control of the algorithm to go down and up to the coarser and finer grids can be done in different ways; the usual one described in [9, 15] is driven by precision tests of the residual on the current grid. We notice that, with such a control, the FAS algorithm can go down and up between two levels for a long time and even never go up to the finest grid for high Reynolds numbers. So, as we solve $L_k(u_k, v_k, p_k) = f_k$ by a relaxation procedure, we use a much simpler control of the algorithm which consists in going down to the coarsest grid before going up, doing a fixed number of iterations on the intermediate grids, then going up to the finest grid. This FAS algorithm is illustrated on Fig. 2.

The full Multigrid algorithm consists in solving the problem with the FAS algorithm on a starting grid G_k $(k \geqslant 1)$ with the test $r_k \leqslant \varepsilon_k$ before going up to a finer grid, then extending this solution to the grid G_{k+1} and so on, until the finest grid. The only control on successive grids is the value of ε_k that is set to

$$\varepsilon_k = \delta \varepsilon_{k+1}, \qquad \delta > 1.$$

In practice for the simplified FMG-FAS procedure we take $\eta = 1.2$ and $\delta = 4$. That means that we allow local divergence between two iterates and require less precision on coarse grids than on fine grids. In addition, we take NBDOWN = 2, NBUP = 1, and NB1 = 10 for a 4×4 coarsest grid (obviously this last number depends on the choice of the coarsest grid). Our experience is that it is not necessary to do numerous iterations of relaxation during the going down or the going up and that 2 and 1 seem to be the best choices to reduce the CPU time. Nevertheless, we need to do more iterations on the coarsest grid to have a good predictor; we can either impose such a fixed number of iterations or require a precision test as follows:

$$\|r_1\| \leqslant \varepsilon_1 = 10^{-2} \|r_l\|.$$

In other words, when we approach the convergence on the finest grid we require $\|r_1\| \leqslant 10^{-2}\varepsilon_l$ on the coarsest grid.

Let us complete this section with the definition of P_{k-1}^k and E_k^{k-1}. These operations represent a tiny part of the CPU time; so we can take good interpolations in order to decrease the number of global iterations on the finest grid. The projection operator is defined by:

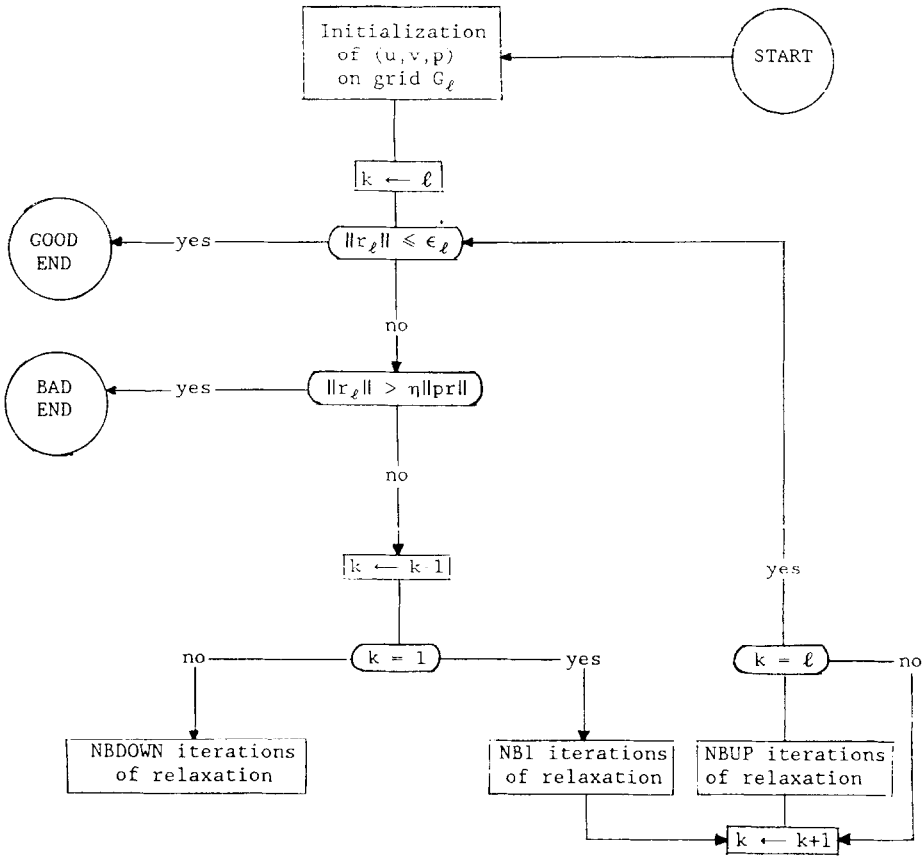

ϵ_ℓ : required precision on grid G_ℓ

r_ℓ : residual on grid G_ℓ

pr : previous residual on grid G_ℓ

η : coefficient of allowed divergence rate.

FIG. 2. Organization chart of simplified FAS.

$$
\begin{cases}
(u_{k-1})_{i-1/2,\,j} = \frac{1}{4}((u_k)_{2i-3/2,\,2j} + (u_k)_{2i-3/2,\,2j-1}) \\
\qquad\qquad + \frac{1}{8}((u_k)_{2i-5/2,\,2j} + (u_k)_{2i-1/2,\,2j} + (u_k)_{2i-5/2,\,2j-1} + (u_k)_{2i-1/2,\,2j-1}) \\
(v_{k-1})_{i,\,j-1/2} = \frac{1}{4}((v_k)_{2i,\,2j-3/2} + (v_k)_{2i-1,\,2j-3/2}) \\
\qquad\qquad + \frac{1}{8}((v_k)_{2i,\,2j-5/2} + (v_k)_{2i,\,2j-1/2} + (v_k)_{2i-1,\,2j-5/2} + (v_k)_{2i-1,\,2j-1/2}) \\
(p_{k-1})_{i,\,j} = \frac{1}{4}((p_k)_{2i-1,\,2j} + (p_k)_{2i,\,2j} + (p_k)_{2i-1,\,2j-1} + (p_k)_{2i,\,2j-1}).
\end{cases}
$$

For the extension operator it is more important to have an accurate interpolation, especially when we extend a converged solution in the FMG procedure; otherwise we lose some information on the finer grid and need more iterations. So the extension operator is defined by:

$$
\begin{aligned}
(u_k)_{2i-3/2,2j-1} = & -\tfrac{3}{128}((u_{k-1})_{i-3/2,j+1} + 2(u_{k-1})_{i-1/2,j+1} + (u_{k-1})_{i+1/2,j+1}) \\
& + \tfrac{15}{64}((u_{k-1})_{i-3/2,j} + 2(u_{k-1})_{i-1/2,j} + (u_{k-1})_{i+1/2,j}) \\
& + \tfrac{5}{128}((u_{k-1})_{i-3/2,j-1} + 2(u_{k-1})_{i-1/2,j-1} + (u_{k-1})_{i+1/2,j-1}) \\
(u_k)_{2i-1/2,2j-1} = & -\tfrac{3}{64}((u_{k-1})_{i-1/2,j+1} + (u_{k-1})_{i+1/2,j+1}) \\
& + \tfrac{15}{32}((u_{k-1})_{i-1/2,j} + (u_{k-1})_{i+1/2,j}) \\
& + \tfrac{5}{64}((u_{k-1})_{i-1/2,j-1} + (u_{k-1})_{i+1/2,j-1}) \\
(v_k)_{2i-1,2j-3/2} = & -\tfrac{3}{128}((v_{k-1})_{i+1,j-3/2} + 2(v_{k-1})_{i+1,j-1/2} + (v_{k-1})_{i+1,j+1/2}) \\
& + \tfrac{15}{64}((v_{k-1})_{i,j-3/2} + 2(v_{k-1})_{i,j-1/2} + (v_{k-1})_{i,j+1/2}) \\
& + \tfrac{5}{128}((v_{k-1})_{i-1,j-3/2} + 2(v_{k-1})_{i-1,j-1/2} + (v_{k-1})_{i-1,j+1/2}) \\
(v_k)_{2i-1,2j-1/2} = & -\tfrac{3}{64}((v_{k-1})_{i+1,j-1/2} + (v_{k-1})_{i+1,j+1/2}) \\
& + \tfrac{15}{32}((v_{k-1})_{i,j-1/2} + (v_{k-1})_{i,j+1/2}) \\
& + \tfrac{5}{64}((v_{k-1})_{i-1,j-1/2} + (v_{k-1})_{i-1,j+1/2}) \\
(p_k)_{2i,2j} = & \tfrac{1}{16}(3(p_{k-1})_{i,j+1} + (p_{k-1})_{i+1,j+1} + 9(p_{k-1})_{i,j} + 3(p_{k-1})_{i+1,j}).
\end{aligned}
$$

3. Relaxation Procedure

In the multigrid technique the choice of the relaxation procedure plays an important role in the efficiency of the method. We use the smoothing operator, proposed in [9], called the symmetrical coupled Gauss–Seidel procedure (SCGS) which consists in a cell by cell under-relaxation procedure. This technique is satisfying because it leads us to solve the problem in a control volume, here a cell, and to update the solution in this control volume. That means, with staggered grids, that the five unknowns of a cell (i, j) are computed simultaneously by solving a 5×5 linear system of the form:

$$
\begin{pmatrix}
a_{11} & 0 & 0 & 0 & 1/\Delta x \\
0 & a_{22} & 0 & 0 & -1/\Delta x \\
0 & 0 & a_{33} & 0 & 1/\Delta y \\
0 & 0 & 0 & a_{44} & -1/\Delta y \\
-1/\Delta x & 1/\Delta x & -1/\Delta y & 1/\Delta y & 0
\end{pmatrix}
\begin{pmatrix}
u_{i-1/2,j} \\ u_{i+1/2,j} \\ v_{i,j-1/2} \\ v_{i,j+1/2} \\ p_{i,j}
\end{pmatrix}
=
\begin{pmatrix}
b_1 \\ b_2 \\ b_3 \\ b_4 \\ b_5
\end{pmatrix}, \qquad (3.1)
$$

TABLE I

Value of the Relaxation Parameter with the Scheme (1.4)–(1.5)

Re	100	400	1000	5000	10,000
Domain $(0.1)\times(0.1)$	1	0.9	0.7	0.3	0.2
Domain $(0.1)\times(0.2)$	0.8	0.3	0.1	—	—

where the diagonal terms contain the diagonal contributions of $D(u, v)$ and $C(u, v)$ and the second members contain all the remaining terms of L_k and the second member f_k. We could have put some other terms in the matrix to intensify the interaction between the unknowns but it seems that such a choice with dominant positive terms on the main diagonal is more efficient. We shall see in the next section how to approximate the convection terms to improve this property. After computing the five unknowns on a cell we update the five corresponding variables by under-relaxation, for instance, we have

$$u^n_{i-1/2,j} = \omega u_{i-1/2,j} + (1-\omega)\, u^{n-1}_{i-1/2,j}; \qquad 0 < \omega \leqslant 1, \tag{3.2}$$

where n is the index of relaxation iterations. Then we solve the problem on the next cell. So, during one iteration, the pressure is updated once and the velocity twice because the components are given on the sides of the cells. In addition we choose a global cell by cell computation from the top to the bottom of the cavity to take immediately into account the driven condition. We conclude this section by giving the value of the optimal under-relaxation parameter ω for various Reynolds numbers in the square cavity and in the rectangular one in Table I. In fact this parameter is closely related to the solution itself, so for a given geometry it depends only on Re but there is a large difference from one geometry to another.

4. Uncentered Schemes for Convection Terms

In this section we analyze in details the influence of the discretization of the convection terms to the computed solution as announced in Section 1. The multigrid procedure with smoothing operator described above gives good efficiency but does not have any influence on the solution. On the contrary the approximation of convection terms has a huge influence on the obtained solution except for small Reynolds numbers ($\mathrm{Re} \leqslant 100$), where every scheme gives a good solution within a few iterations; even the centered scheme written for $u_{i-1/2,j}$ and $v_{i,j-1/2}$,

$$[C_k(u,v)]_{(i,j)} = \begin{cases} \dfrac{u_{i-1/2,j}}{2\,\Delta x}\,(u^{n-1}_{i+1/2,j} - u^{n-1}_{i-3/2,j}) + \dfrac{v^{n-1}_{i-1/2,j}}{2\,\Delta y}\,(u^{n-1}_{i-1/2,j+1} - u^{n-1}_{i-1/2,j-1}) \\ \dfrac{u^{n-1}_{i,j-1/2}}{2\,\Delta x}\,(v^{n-1}_{i+1,j-1/2} - v^{n-1}_{i-1,j-1/2}) + \dfrac{v_{i,j-1/2}}{2\,\Delta y}\,(v^{n-1}_{i,j+1/2} - v^{n-1}_{i,j-3/2}), \end{cases} \tag{4.1}$$

where the unknown values $u^{n-1}_{i,j-1/2}$ and $v^{n-1}_{i-1/2,j}$ are computed by linear interpolation of the four known neighbours. Replacing formula (1.5), this formula completes formulas (1.4); we see that it adds terms on the main diagonal of matrix (3.1) with a positive or negative sign according to the sign of $u^{n-1}_{i+1/2,j} - u^{n-1}_{i-3/2,j}$ and $v^{n-1}_{i,j+1/2} - v^{n-1}_{i,j-3/2}$. This plays a significant role in the behaviour of the centered scheme that is good for small Reynolds numbers but very unstable and dispersive as soon as Re increases. Moreover, the centered scheme does not take into account the hyperbolic behaviour of the convection terms. So for these terms the first idea is to use an upwind scheme given for the first unknown $u_{i-1/2,j}$ by:

$$\begin{cases} \dfrac{u^{n-1}_{i-1/2,j}}{\Delta x}\,(u_{i-1/2,j} - u^{n-1}_{i-3/2,j}) & \text{if } u^{n-1}_{i-1/2,j} > 0 \\ \dfrac{u^{n-1}_{i-1/2,j}}{\Delta x}\,(u^{n-1}_{i+1/2,j} - u_{i-1/2,j}) & \text{otherwise} \end{cases}$$

$$+ \begin{cases} \dfrac{v^{n-1}_{i-1/2,j}}{\Delta y}\,(u_{i-1/2,j} - u^{n-1}_{i-1/2,j-1}) & \text{if } v^{n-1}_{i-1/2,j} > 0 \\ \dfrac{v^{n-1}_{i-1/2,j}}{\Delta y}\,(u^{n-1}_{i-1/2,j+1} - u_{i-1/2,j}) & \text{otherwise.} \end{cases} \tag{4.2}$$

Now this scheme is sensitive to the propagation of the information with hyperbolic terms and, besides, the additional terms on the main diagonal of the matrix (3.1) are always positive. Consequently this scheme is stable for high Reynolds numbers but, as it is often the case for uncentered first-order schemes (see, for instance, [17]) it is very diffusive. So both the location and the amplitude of the extrema of the velocity profiles are uncorrect as shown on Fig. 3 for Re = 1000 on a medium 64×64 grid.

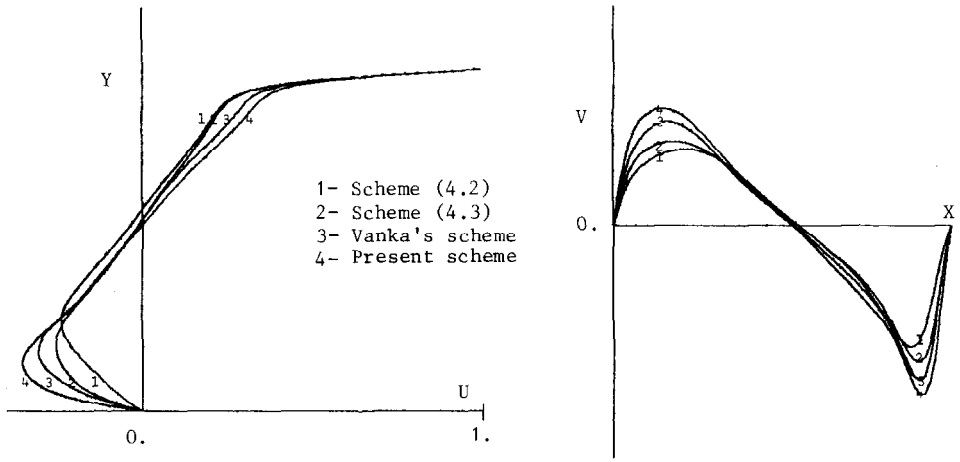

FIG. 3. Comparison of different schemes on velocity profiles, Re = 1000, grid 64×64.

At this stage we see that we have to find an intermediate scheme both stable and able to capture correctly the solution as soon as there are enough points to represent it. In order to improve the location of the phenomena we write another uncentered first-order scheme sensitive to the solution in the neighbourhood of the cell (i, j); that is, for $u_{i-1/2,j}$,

$$\begin{cases} \dfrac{u^{n-1}_{i-1,j}}{\Delta x}\,(u_{i-1/2,j} - u^{n-1}_{i-3/2,j}) & \text{if } u^{n-1}_{i-1,j} > 0 \\ + \dfrac{u^{n-1}_{i,j}}{\Delta x}\,(u^{n-1}_{i+1/2,j} - u_{i-1/2,j}) & \text{if } u^{n-1}_{i,j} < 0 \end{cases}$$

$$+ \begin{cases} \dfrac{v^{n-1}_{i-1/2,j-1/2}}{\Delta y}\,(u_{i-1/2,j} - u^{n-1}_{i-1/2,j-1}) & \text{if } v^{n-1}_{i-1/2,j-1/2} > 0 \\ + \dfrac{v^{n-1}_{i-1/2,j+1/2}}{\Delta y}\,(u^{n-1}_{i-1/2,j+1} - u_{i-1/2,j}) & \text{if } v^{n-1}_{i-1/2,j+1/2} < 0, \end{cases} \tag{4.3}$$

where $u^{n-1}_{i-1,j}$, $u^{n-1}_{i,j}$, $v^{n-1}_{i-1/2,j-1/2}$, and $v^{n-1}_{i-1/2,j+1/2}$ can be seen as the mean component of the velocity in a left, right, bottom, and top cell of the current point $(i-1/2, j)$, respectively. This scheme, inspired by Murman's, is much more stable than the previous one and gives a quite good location of the extrema of velocity profiles (see Fig. 3) but, unfortunately, it needs many points to get the right amplitude as the scheme (4.2). We can remark that the convection terms in (4.3) are not written at point $(i-1/2, j)$ but at points $(i-1, j)$, (i, j), $(i-1/2, j-1/2)$, and $(i-1/2, j+1/2)$ instead; then the derivatives in these terms are approximated by centered second-order differences at these points.

We propose finally to replace these derivatives by uncentered second-order differences at these neighbouring points. Let us denote by x one of these points; we can write Taylor's formulas:

$$\begin{aligned} u(x-h/2) &= u(x) - h/2u'(x) + h^2/8u''(x) + O(h^3) \\ u(x-3h/2) &= u(x) - 3h/2u'(x) + 9h^2/8u''(x) + O(h^3). \end{aligned} \tag{4.4}$$

From (4.4) we have

$$u'(x) = \frac{8u(x) - 9u(x-h/2) + u(x-3h/2)}{3h} + O(h^2),$$

and with linear interpolation of the unknown value $u(x)$ we find for the first derivative:

$$u'(x) = \frac{4u(x+h/2) - 5u(x-h/2) + u(x-3h/2)}{3h}. \tag{4.5}$$

Instead of (4.4) or in addition to (4.4) we could have written Taylor's series for $u(x-h)$ and $u(x+h/2)$; then we get many possible combinations to determine the first derivative with a second or third order of accuracy. Among all these possibilities the good formulas have the form:

$$u'(x)=\frac{\alpha u(x+h/2)-(\alpha+1)\,u(x-h/2)+u(x-3h/2)}{(\alpha-1)\,h} \qquad \text{with} \quad \alpha=3,\,4,\,5,\,7,\,13;$$

the two latest are of third order. These formulas correspond to introducing an anti-diffusion term $(h\,|u|/(\alpha-1))\,u''(x)$, which reduces the artificial diffusion contained in the first-order scheme (4.3). For $\alpha=3$ the resulting scheme is very unstable even with small relaxation parameters. On the contrary, all the other values of α yield a stable scheme that gives better results than (4.3). Thus, as α increases, the scheme is more stable and the results are not as good because there is more and more artificial diffusion in the scheme; the case $\alpha=4$ can be seen as a limit of stability and, as is often the case, gives the best results. Finally, the value $\alpha=4$ yields the proposed scheme (1.5).

In Fig. 3 we compare this scheme with (4.2) and (4.3) schemes and those used by Vanka in [9]. We see that for $\mathrm{Re}=1000$ and a medium mesh of 64×64 cells the scheme (1.5) gives a good location and amplitude of the extrema of velocity profiles. The results on a finer mesh are in good agreement with the results presented in [8–10, 14] as shown in Table II, although the secondary vortices are larger with the present scheme; we think that this is due to the fact that our scheme is less

TABLE II

Comparison of Solutions for $\mathrm{Re}=1000$

Extrema of velocity profiles along centerlines

	$u_{\min}$	$y_{\min}$	$v_{\max}$	$x_{\max}$	$v_{\min}$	$x_{\min}$
Ghia, Ghia, and Shin	−0.3829	0.1719	0.3709	0.1563	−0.5155	0.9063
Vanka ([a])	−0.3798	0.1680	0.3669	0.1563	−0.5186	0.9102
Zhang	−0.3901	0.1699	0.3785	0.1582	−0.5284	0.9082
Present method ([a])	−0.3764	0.1602	0.3665	0.1523	−0.5208	0.9102

Extrema of stream function

	Primary vortex		Secondary vortex bottom right		Secondary vortex bottom left	
	Φ	(location)	Φ	(location)	Φ	(location)
Ghia, Ghia, and Shin	−0.1179	(0.5313, 0.5625)	0.175E-2	(0.8594, 0.1094)	0.231E-3	(0.0859, 0.0781)
Schreiber and Keller	−0.1160	(0.5286, 0.5643)	0.170E-2	(0.8643, 0.1071)	0.217E-3	(0.0857, 0.0714)
Vanka ([a])	−0.1138	(0.5313, 0.5664)	0.164E-2	(0.8672, 0.1133)	0.238E-3	(0.0820, 0.0781)
Zhang	−0.1193	(0.5313, 0.5664)	0.174E-2	(0.8633, 0.1133)	0.235E-3	(0.0820, 0.0781)
Present method ([a])	−0.1163	(0.5313, 0.5586)	0.191E-2	(0.8711, 0.1094)	0.325E-3	(0.0859, 0.0820)

[a] Results computed in this work on a 256×256 grid.

diffusive. Moreover, we see in Fig. 4 that the results obtained on the 64×64 mesh are already closed to the solution and closer than those obtained with Vanka's scheme (Fig. 3). In this last scheme the diffusion term and the convection term are closely linked and the diffusion term is suppressed as soon as the convection term prevails. We can write $[D_k(u, v)]_{(i,j)} + [C_k(u, v)]_{(i,j)}$ for the unknown $u_{i-1/2,j}$ as

$$\begin{cases} \dfrac{(u_{i-1/2,j} - u^{n-1}_{i-3/2,j})}{\mathrm{Re}(\Delta x)^2} + \dfrac{u^{n-1}_{i-1,j}}{2\,\Delta x}(u_{i-1/2,j} - u^{n-1}_{i-3/2,j}) & \text{if } \left|\dfrac{u^{n-1}_{i-1,j}}{2\,\Delta x}\right| < \dfrac{1}{\mathrm{Re}(\Delta x)^2} \\ \left(\left|\dfrac{u^{n-1}_{i-1,j}}{2\,\Delta x}\right| + \dfrac{u^{n-1}_{i-1,j}}{2\,\Delta x}\right)(u_{i-1/2,j} - u^{n-1}_{i-3/2,j}) & \text{otherwise} \end{cases}$$

$$+ \begin{cases} \dfrac{(u_{i-1/2,j} - u^{n-1}_{i+1/2,j})}{\mathrm{Re}(\Delta x)^2} + \dfrac{u^{n-1}_{i,j}}{2\,\Delta x}(u^{n-1}_{i+1/2,j} - u_{i-1/2,j}) & \text{if } \left|\dfrac{u^{n-1}_{i,j}}{2\,\Delta x}\right| < \dfrac{1}{\mathrm{Re}(\Delta x)^2} \\ \left(\left|\dfrac{u^{n-1}_{i,j}}{2\,\Delta x}\right| - \dfrac{u^{n-1}_{i,j}}{2\,\Delta x}\right)(u_{i-1/2,j} - u^{n-1}_{i+1/2,j}) & \text{otherwise} \end{cases}$$

$$+ \begin{cases} \dfrac{(u_{i-1/2,j} - u^{n-1}_{i-1/2,j-1})}{\mathrm{Re}(\Delta y)^2} + \dfrac{v^{n-1}_{i-1/2,j-1/2}}{2\,\Delta y}(u_{i-1/2,j} - u^{n-1}_{i-1/2,j-1}) & \text{if } \left|\dfrac{v^{n-1}_{i-1/2,j-1/2}}{2\,\Delta y}\right| < \dfrac{1}{\mathrm{Re}(\Delta y)^2} \\ \left(\left|\dfrac{v^{n-1}_{i-1/2,j-1/2}}{2\,\Delta y}\right| + \dfrac{v^{n-1}_{i-1/2,j-1/2}}{2\,\Delta y}\right)(u_{i-1/2,j} - u^{n-1}_{i-1/2,j-1}) & \text{otherwise} \end{cases}$$

$$+ \begin{cases} \dfrac{(u_{i-1/2,j} - u^{n-1}_{i-1/2,j+1})}{\mathrm{Re}(\Delta y)^2} + \dfrac{v^{n-1}_{i-1/2,j+1/2}}{2\,\Delta y}(u^{n-1}_{i-1/2,j+1} - u_{i-1/2,j}) & \text{if } \left|\dfrac{v^{n-1}_{i-1/2,j+1/2}}{2\,\Delta y}\right| < \dfrac{1}{\mathrm{Re}(\Delta y)^2} \\ \left(\left|\dfrac{v^{n-1}_{i-1/2,j+1/2}}{2\,\Delta y}\right| - \dfrac{v^{n-1}_{i-1/2,j+1/2}}{2\,\Delta y}\right)(u_{i-1/2,j} - u^{n-1}_{i-1/2,j+1}) & \text{otherwise,} \end{cases}$$

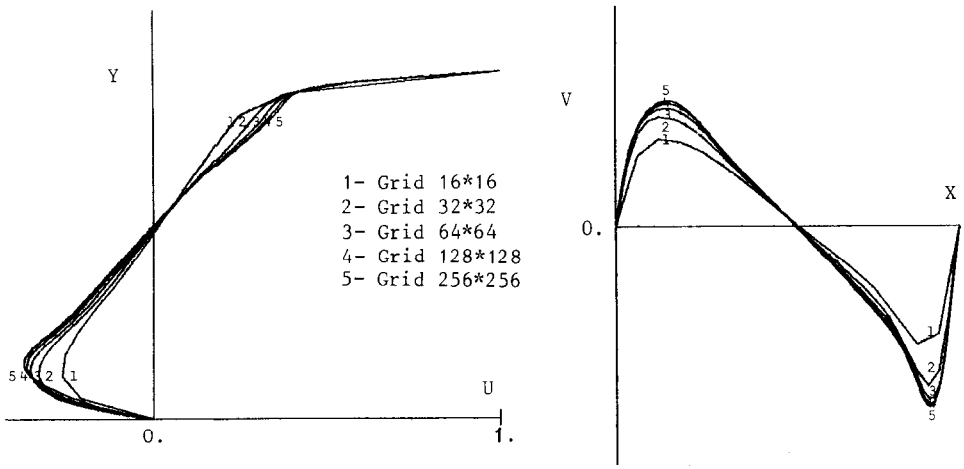

FIG. 4. Evolution of velocity profiles along centerlines with different grids, $\mathrm{Re} = 1000$.

where $u^{n-1}_{i-1,j}$, $u^{n-1}_{i,j}$, $v^{n-1}_{i-1/2,j-1/2}$, and $v^{n-1}_{i-1/2,j+1/2}$ are defined as in (4.3). We see that this scheme is a good intermediate between the centered scheme (4.1) and the scheme (4.3), which could be the key of its success. Nevertheless, the suppression of the diffusion term in some cases can decrease its stability and explain the difficulties to get the solution for Reynolds number equal to 5000. To close this section we add that the scheme presented in [14] is the same as (4.2) with a second-order approximation of the derivatives of the form

$$u'(x) = \frac{3u(x) - 4u(x-h) + u(x-2h)}{2h}.$$

It gives good results but is not very stable, either, as we have seen above for $\alpha = 3$.

We do not pretend to make an exhaustive discussion about the schemes but hope to shed some light on the difficult problem of the approximation of convection terms.

We close this section by giving the extrapolation at the boundary; as the scheme (1.4)–(1.5) uses second-order derivatives we take a parabolic extrapolation written for the unknown u on the left-hand side as follows:

$$u_{-1/2,j} = 3u_{1/2,j} - 3u_{3/2,j} + u_{5/2,j}$$

and, at the bottom,

$$u_{i-1/2,0} = \tfrac{8}{3}u_{i-1/2,1/2} - 2u_{i-1/2,1} + \tfrac{1}{3}u_{i-1/2,2}$$

$$u_{i-1/2,-1} = 8u_{i-1/2,1/2} - 9u_{i-1/2,1} + 2u_{i-1/2,2}.$$

This extrapolation improves the representation of the boundary conditions and gives better results on coarse grids. But on fine meshes the first-order extrapolation yields about the same results.

5. Numerical Results

In this section we comment on some results in the square-driven cavity and in the rectangular cavity of the ratio-two aspect. These results are obtained with the simplified FMG-FAS algorithm and the finite differences schemes (1.4)–(1.5). Generally, the solution is initialized by zero on the starting grid of the FMG algorithm; but in some cases, particularly for high Reynolds numbers, it is initialized on this grid with the solution obtained for a lower Reynolds number. The pressure is also initialized by zero everywhere and is not fixed at any point. Indeed we know that the pressure is determined within a constant but this constant is given by the initialization; the relaxation procedure allows us to let the pressure free without getting overshoots. In fact, the results show that the pressure, in this case of zero initialization, is always less than one.

TABLE III

Comparison of Efficiency with Vanka's Scheme

	128 × 128 grid			256 × 256 grid		
	ω optimal	Number of iterations	CPU time (seconds)	ω optimal	Number of iterations	CPU time
Vanka	0.6	20	53	0.5	10	1 min 41 s
Present method	0.7	7	24	0.7	6	1 min 10 s

First, we compare the efficiency of the present method with other methods. For $Re = 1000$ we get the solution on a 128×128 grid in only 24 s of SIEMENS VP 200. In [10] with a stream function-vorticity formulation the same test requires

[redacted]

because we have tested both of them. In Table III we give a comparison for $Re = 1000$ on a 128×128 grid with the simplified FMG-FAS algorithm and on a 256×256 grid with FAS algorithm and initialization by the solution obtained on the previous grid. We notice that the scheme (1.4)–(1.5) is approximately twice as

TABLE IV

Extrema of Velocity Profiles along Centerlines and Stream Functions

Re		100		1000		5000	
$u_{\min}$	$y_{\min}$	−0.2106	0.4531	−0.3764	0.1602	−0.4359	0.0664
$v_{\max}$	$x_{\max}$	0.1786	0.2344	0.3665	0.1523	0.4259	0.0762
$v_{\min}$	$x_{\min}$	−0.2521	0.8125	−0.5208	0.9102	−0.5675	0.9590
Primary vortex - Φ (location)		−0.1026	(0.6172, 0.7344)	−0.1163	(0.5313, 0.5586)	−0.1142	(0.5156, 0.5313)
Second. vortex bottom right Φ (location)		0.123E-4	(0.9453, 0.0625)	0.191E-2	(0.8711, 0.1094)	0.465E-2	(0.8301, 0.0703)
Second. vortex bottom left Φ (location)		0.163E-5	(0.0313, 0.0391)	0.325E-3	(0.0859, 0.0820)	0.222E-2	(0.0664, 0.1484)
Second. vortex top left Φ (location)			—	0.755E-3	(0.0039, 1.0000)	0.175E-2	(0.0625, 0.9102)
Tertiary vortex bottom right Φ (location)			—		—	−0.247E-4	(0.9668, 0.0293)
Tertiary vortex bottom left Φ (location)			—	−0.306E-8	(0.0039, 0.0039)	−0.233E-6	(0.0117, 0.0098)

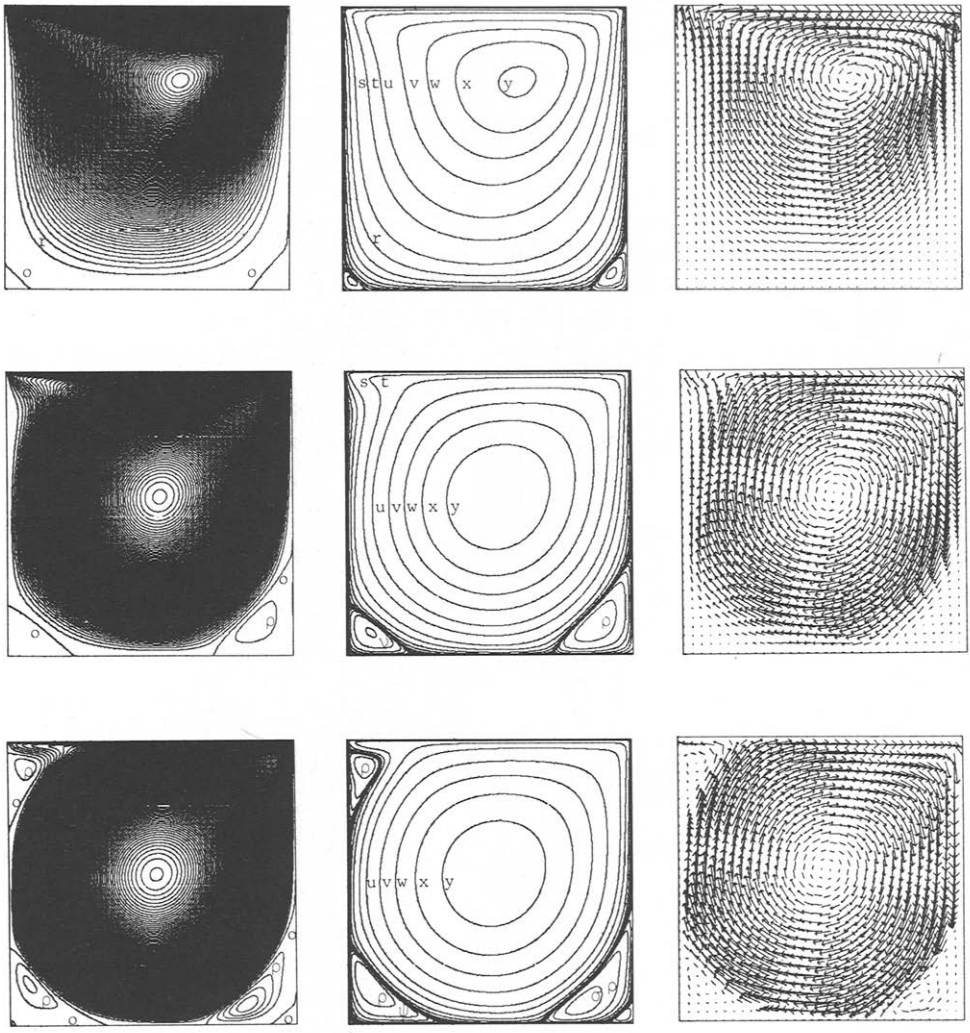

FIG. 5. Equidistant streamlines, tabulated streamlines, and velocity fields in the square cavity, Re = 100, 1000, and 5000.

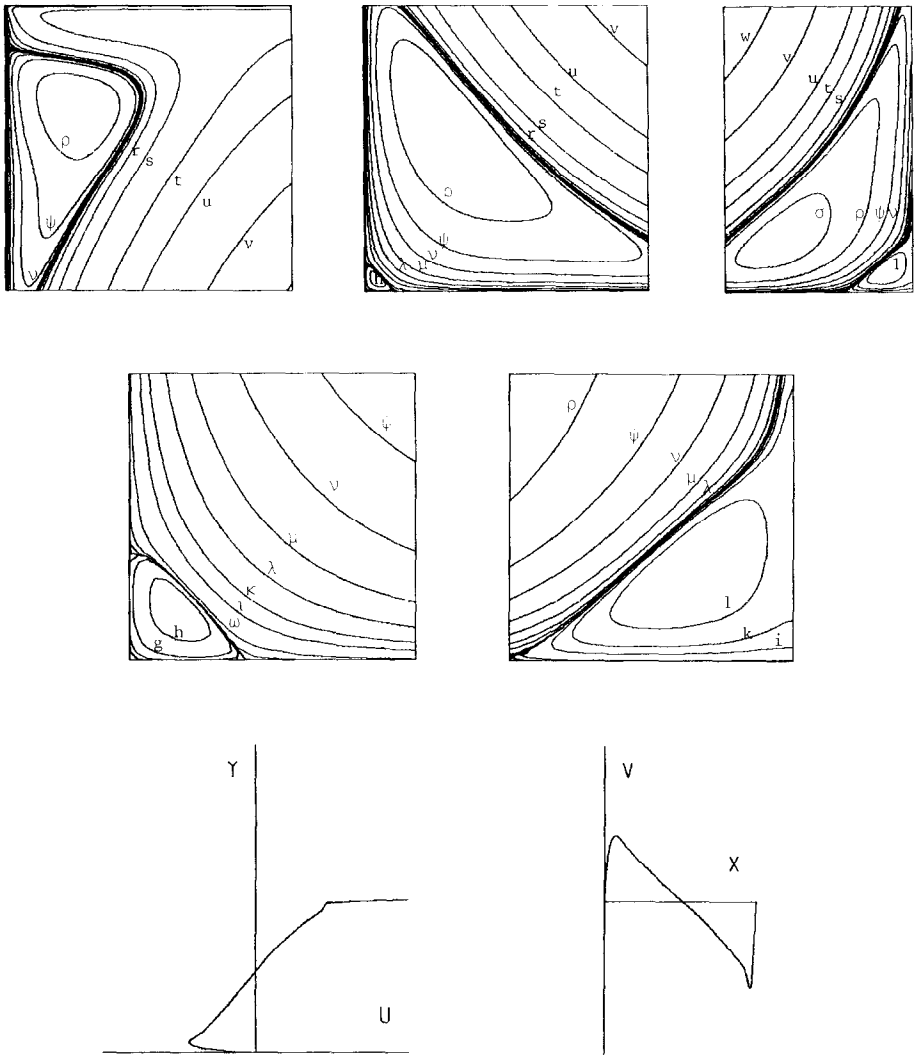

FIG. 6. Details of the solution for Re = 5000: secondary vortices; tertiary vortices; velocity profiles along centerlines.

fast as Vanka's scheme on the 128×128 grid and that the optimal relaxation parameter is larger.

Table IV gives the main characteristics of the solution for $Re = 100$ on a 128×128 grid, $Re = 1000$ on a 256×256 grid, and $Re = 5000$ on a 512×512 grid. In every case we observe a good convergence to the steady laminar solution with a residual r_l less than 10^{-4}. Let us notice that, in the three cases, we represent the solution on the finest grid reached by the FMG algorithm that stops when the solution does not change noticeably. The solution depends on the grid when the grids are coarse and is independent when the grids are finer. For instance, this is illustrated in Fig. 4, where we see that the solution is quite different on the coarse grids until 64×64 and then is the same on the grids 128×128 and 256×256. In this case the grid 256×256 is very fine with respect to Reynolds number 1000 but confirms the stability of the solution. We can affirm that we get a steady laminar solution until $Re = 5000$.

Moreover, in accordance with [8], the minimum of the stream function increases between $Re = 1000$ and $Re = 5000$. In Figs. 5 and 6 these solutions are plotted in the square cavity with details of secondary and tertiary vortices for $Re = 5000$. The streamlines plotted on the figures are either equidistant with a step of 10^{-3} (the separation lines represented by level zero are denoted by 0) or fixed to forty given values. These values are listed in Table V.

Now we notice a very interesting behaviour of the computation process for $Re = 7500$ and $Re = 10{,}000$. Indeed, on coarse grids (until 128×128 for $Re = 10{,}000$) there is no convergence of the residual; on the 256×256 grid there is a good convergence to a steady laminar solution (Fig. 7) and on the finer 512×512 grid there is no convergence any more (the residual decreases at the beginning and then oscillates around a value) and apparition of new small eddies (Fig. 8). In this late case the relaxation procedure can be seen like a time procedure, and then we

TABLE V

Values of the Streamlines

Contour letter	Value of Φ	Contour letter	Value of Φ	Contour letter	Value of Φ	Contour letter	Value of Φ
y	−0.1	t	−1.E-2	e	−1.E-10	ζ	1.E-9
x	−0.08	s	−3.E-3	d	−1.E-11	η	1.E-8
w	−0.06	r	−1.E-3	c	−1.E-12	ω	1.E-7
v	−0.04	p	−3.E-4	b	−1.E-13	ι	1.E-6
u	−0.02	n	−1.E-4	a	−1.E-14	κ	3.E-6
		m	−3.E-5	o	0	λ	1.E-5
		l	−1.E-5	α	1.E-14	μ	3.E-5
		k	−3.E-6	β	1.E-13	ν	1.E-4
		i	−1.E-6	γ	1.E-12	ψ	3.E-4
		h	−1.E-7	δ	1.E-11	ρ	1.E-3
		g	−1.E-8	ε	1.E-10	σ	3.E-3
		f	−1.E-9			τ	1.E-2

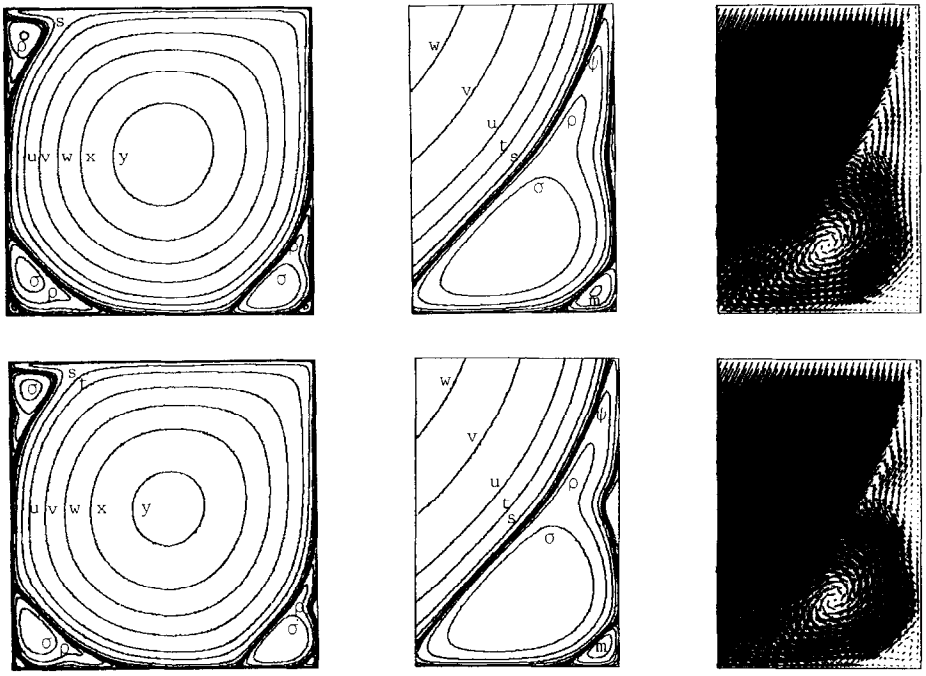

FIG. 7. Converged solutions with the 256×256 grid, $\mathrm{Re} = 7500$ and 10,000.

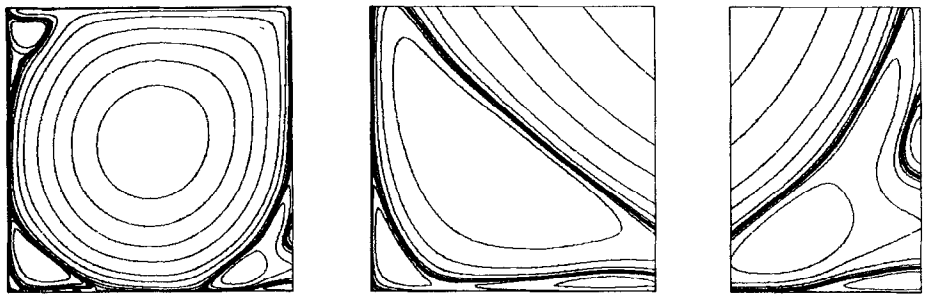

FIG. 8. Small perturbations along the walls in the corners for $\mathrm{Re} = 7500$ with the 512×512 grid.

observe an evolution of the small eddies along the walls. Our explanation for this behaviour is the following: if there is no points in the boundary layer, the solution cannot be represented properly and the method does not converge. We know that the thickness of the boundary layer is of the order of $1/\sqrt{\text{Re}}$; so this explains the non convergence on coarse grids. For smaller values of the mesh size the process converges to the steady laminar solution if it exists; this is the case for $\text{Re} = 5000$, for instance. But, as we use a steady model, the method can converge artificially on quite fine grids as long as the mesh size is not fine enough to take into account the instabilities. This is the case for $\text{Re} = 7500$ and $\text{Re} = 10{,}000$ on the 256×256 grid. The Kolmogorov length is of the order of $1/\text{Re}^{3/4}$ and according to Kolmogorov and [5] we need a mesh size as small as this to capture the turbulence. So it seems that there is no laminar solution any more for these two Reynolds numbers and that, as soon as the mesh size is small enough to represent the phenomena, the method cannot converge. We see that the converged solutions on the 256×256 grid exhibit small eddies along the wall in addition to the usual secondary and tertiary vortices in the corners (the main characteristics of these solutions are listed in Table VI). Then unstable flow on the grid 512×512 for $\text{Re} = 10{,}000$ is plotted on Fig. 9.

Now starting with the solution obtained on the 256×256 grid for $\text{Re} = 10{,}000$, we run the code on this grid for higher Reynolds numbers up to 15,000. Then we see small eddies developing along the walls which move during the iterations as shown on Fig. 10 for $\text{Re} = 11{,}000$ and the apparition of strange structures like a double center vortex for $\text{Re} = 15{,}000$ (Fig. 11). Finally, we conjecture that beyond

TABLE VI

Extrema of Velocity Profiles along Centerlines and Stream Functions of the Solution with the 256×256 Grid

Re		7500		10,000	
$u_{\min}$	$y_{\min}$	−0.4379	0.0508	−0.4373	0.0430
$v_{\max}$	$x_{\max}$	0.4179	0.0625	0.4141	0.0547
$v_{\min}$	$x_{\min}$	−0.5640	0.9688	−0.5610	0.9727
Primary vortex Φ (location)		−0.1113	(0.5156, 0.5234)	−0.1053	(0.5156, 0.5234)
Second. vortex bottom right Φ (location)		0.832E-2	(0.8828, 0.0820)	0.986E-2	(0.8945, 0.0820)
Second. vortex bottom left Φ (location)		0.476E-2	(0.0703, 0.1289)	0.623E-2	(0.0781, 0.1133)
Second. vortex top left Φ (location)		0.314E-2	(0.0664, 0.9141)	0.403E-2	(0.0664, 0.9141)

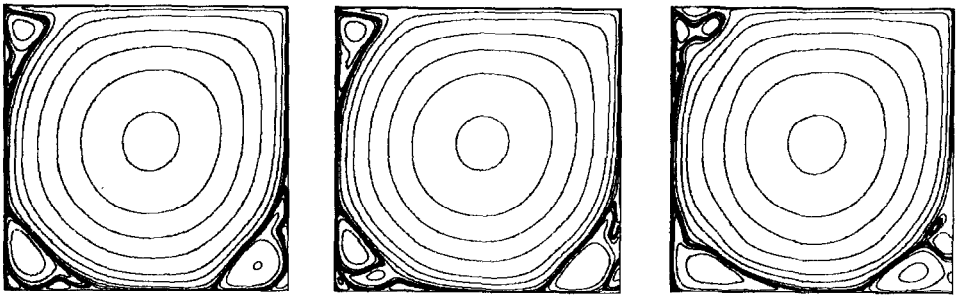

FIG. 9. Evolution of the solution during iterations for $Re = 10{,}000$ with the 512×512 grid.

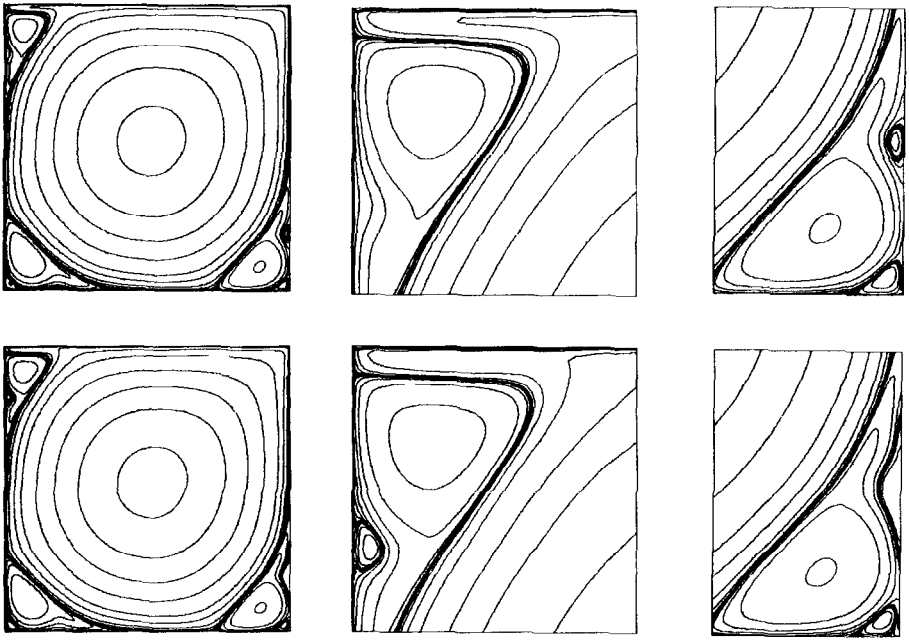

FIG. 10. Appearance and disappearance of small eddies for $Re = 11{,}000$ with the 256×256 grid, 50 and 150 iterations.

FIG. 11. Solution after 150 iterations for $Re = 15{,}000$ with the 256×256 grid.

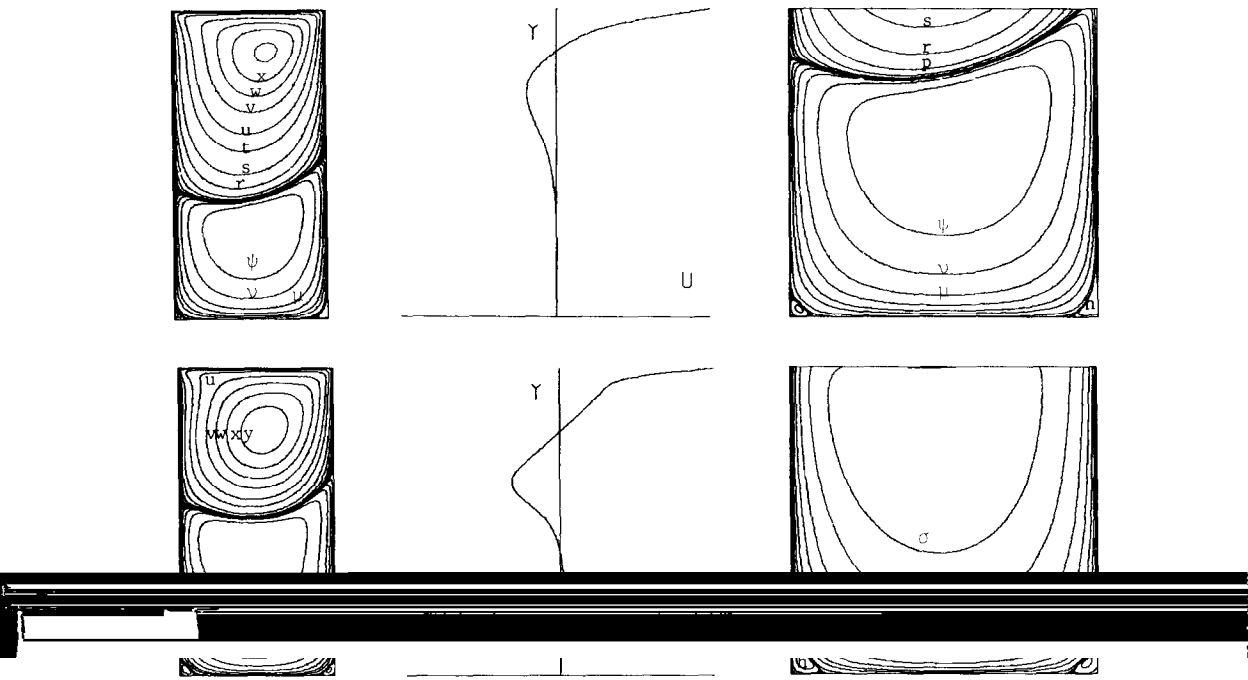

FIG. 12. Streamlines and u velocity profile along centerline in the rectangular cavity, $Re = 100$ and 400.

TABLE VII

Extrema of u Velocity Profile along Centerline and Stream Function

Re		100		400		1000	
u_{min}	y_{min}	−0.1968	1.4531	−0.3146	1.2578	−0.3851	1.1680
u_{max}	y_{max}	0.00195	0.3438	0.01781	0.5703	0.03102	0.5
Primary vortex top Φ (location)		−0.1033	(0.6172, 1.7344)	−0.1124	(0.5547, 1.5938)	−0.1169	(0.5273, 1.5625)
Primary vortex bottom Φ (location)		0.783E-3	(0.5391, 0.5859)	0.909E-2	(0.4297, 0.8125)	0.0148	(0.3516, 0.7891)
Second. vortex bottom left Φ (location)		−0.149E-7	(0.0313, 0.0313)	−0.257E-6	(0.0391, 0.0469)	−0.108E-4	(0.0977, 0.1094)
Second. vortex bottom right[a] Φ (location)		−0.335E-6	(1.0000, 0.3750)	−0.146E-6	(0.9688, 0.0391)	−0.459E-4	(1.0000, 0.3750)

[a] This last vortex is quite unstable during iterations.

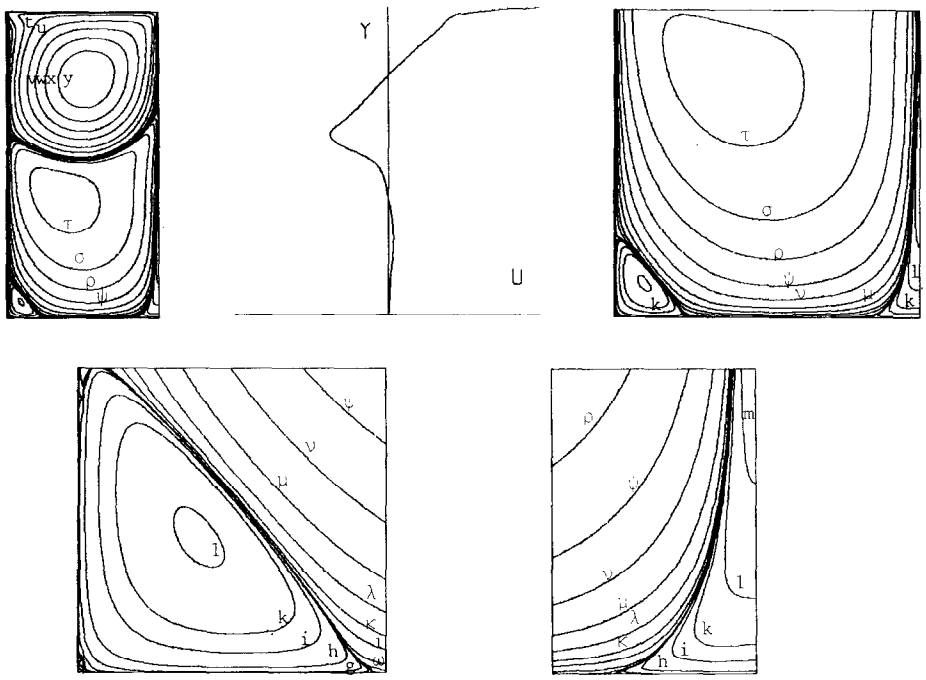

FIG. 13. Streamlines and u velocity profile along centerline in the rectangular cavity, Re = 1000.

$\mathrm{Re} = R_c$ with $5000 < R_c < 7500$ there is not a steady laminar solution any more and the transition to turbulence occurs when small eddies develop along the walls.

Let us conclude this section with some results in the rectangular cavity of aspect ratio equal to two. The main results are listed in Table VII for $\mathrm{Re} = 100$ and 400 on a uniform 128×256 grid and for $\mathrm{Re} = 1000$ on a 256×512 grid. Illustrations are plotted on Figs. 12 and 13. We notice, as indicated in Table I, that the optimal relaxation parameter is very small with respect to the square cavity. We believe that this limit of stability is due to the complexity of the solution in this case and that the transition to turbulence should appear for R_c quite close to 1000. In [13] a Hopf bifurcation is expected in this cavity for $2000 \leqslant R_c \leqslant 10{,}000$.

CONCLUSION

In this work a new scheme for the discretization of convection terms of Navier–Stokes equations is proposed. Coupled with a simplified FMG-FAS algorithm and a cell by cell relaxation procedure this scheme is very stable and efficient. The steady laminar solution is computed for $\mathrm{Re} = 1000$ on a 128×128 grid in 24 s and for $\mathrm{Re} = 5000$ on a 512×512 grid in half an hour of CPU time on a SIEMENS VP 200.

The results are in good agreement with other published results in the square driven cavity for Reynolds number less or equal to 1000. The solutions computed in this work exhibit a very good representation of secondary and tertiary vortices. It appears that the solution is laminar for $\mathrm{Re} \leqslant 5000$ and becomes unstable for the steady model with $\mathrm{Re} = 7500$ on the fine 512×512 grid when small eddies develop along the walls in the corners. We hope to confirm these results with further works on the unsteady Navier–Stokes equations.

Finally, some results are given in the rectangular driven cavity of aspect ratio equal to two and a parallel is made with results obtained in the square cavity. It seems that the flow is much more complex in the rectangular cavity and the limit of stability is reached in this case for $\mathrm{Re} = 1000$ although a steady laminar solution is still captured for this Reynolds number.

REFERENCES

1. M. FORTIN, R. PEYRET, AND R. TEMAM, *J. Mec.* **10**, 357 (1971).
2. F. THOMASSET, *Implementation of Finite Element Methods for Navier–Stokes Equations* (Springer-Verlag, New York/Heidelberg/Berlin, 1981).
3. R. PEYRET AND T. D. TAYLOR, *Computational Methods for Fluid Flow* (Springer-Verlag, New York/Heidelberg/Berlin, 1983).
4. A. FORTIN, M. FORTIN, AND J. J. GERVAIS, *J. Comput. Phys.* **70**, 295 (1987).
5. P. CONSTANTIN, C. FOIAS, AND R. TEMAM, Attractors representing turbulent flows, *Mem. Amer. Math. Soc.* **53**, 314 (1985).
6. P. LE QUERE AND T. ALZIARY DE ROQUEFORT, *J. Comput. Phys.* **57**, 210 (1985).

7. J. SHEN, Thesis, University of Paris-Sud, Orsay, 1987 (unpublished).
8. R. SCHREIBER AND H. B. KELLER, *J. Comput. Phys.* **49**, 310 (1983).
9. S. P. VANKA, *J. Comput. Phys.* **65**, 138 (1986).
10. U. GHIA, K. N. GHIA, AND C. T. SHIN, *J. Comput. Phys.* **48**, 387 (1982).
11. H. K. MOFFATT, *J. Fluid Mech.* **18**, 1 (1964).
12. K. GUSTAFSON AND R. LEBEN, *Appl. Math. Comput.* **19**, 89 (1986).
13. K. GUSTAFSON AND K. HALASI, *J. Comput. Phys.* **70**, 271 (1987).
14. L. B. ZHANG, Thesis, University of Paris-Sud, Orsay, 1987 (unpublished).
15. A. BRANDT AND N. DINAR, in *Proceedings of an Advanced Seminar Conducted by the Mathematical Research Center*, The University of Wisconsin-Madison, 1978, edited by S. V. Parter (Academic Press, New York/London, 1979), p. 53.
16. W. HACKBUSCH, *Multigrid Methods and Applications* (Springer-Verlag, New York/Heidelberg/Berlin, 1985).
17. D. B. SPALDING, *Int. J. Num. Meth. Eng.* **4**, 551 (1972).